

# Metal-to-metal transition and heavy-electron state in $\text{Nd}_4\text{Ni}_3\text{O}_{10-\delta}$

Bai-Zhuo Li,<sup>1</sup> Cao Wang,<sup>2</sup> P. T. Yang,<sup>3,4</sup> J. P. Sun,<sup>3,4</sup> Ya-Bin Liu,<sup>1</sup> Jifeng Wu,<sup>5</sup>  
Zhi Ren,<sup>5</sup> J. -G. Cheng,<sup>3,4,6</sup> Guang-Ming Zhang,<sup>7</sup> and Guang-Han Cao<sup>1,8,\*</sup>

<sup>1</sup>*Department of Physics, Zhejiang Province Key Laboratory of Quantum Technology and Devices,  
Interdisciplinary Center for Quantum Information,  
and State Key Lab of Silicon Materials, Zhejiang University, Hangzhou 310027, China*

<sup>2</sup>*School of Physics & Optoelectronic Engineering,  
Shandong University of Technology, Zibo 255000, China*

<sup>3</sup>*Beijing National Laboratory for Condensed Matter Physics and Institute of Physics,  
Chinese Academy of Sciences, Beijing, 100190, China*

<sup>4</sup>*School of Physical Sciences, University of Chinese Academy of Sciences, Beijing 100190, China*

<sup>5</sup>*School of Science, Westlake Institute for Advanced Study, Westlake University, Hangzhou 310064, China*

<sup>6</sup>*Songshan Lake Materials Laboratory, Dongguan, Guangdong 523808, China*

<sup>7</sup>*State Key Laboratory of Low-Dimensional Quantum Physics and  
Department of Physics, Tsinghua University, Beijing 100084, China*

<sup>8</sup>*Collaborative Innovation Centre of Advanced Microstructures, Nanjing 210093, China*

(Dated: February 12, 2020)

The trilayer nickelate  $\text{Nd}_4\text{Ni}_3\text{O}_{10-\delta}$  ( $\delta \approx 0.15$ ) was investigated by the measurements of x-ray diffraction, electrical resistivity, magnetic susceptibility, and heat capacity. The crystal structure data suggest a higher Ni valence in the inner perovskite-like layer. At ambient pressure the resistivity shows a jump at 162 K, indicating a metal-to-metal transition (MMT). The MMT is also characterized by a magnetic susceptibility drop, a sharp specific-heat peak, and an isotropic lattice contraction. Below  $\sim 50$  K, a resistivity upturn with a  $\log T$  dependence shows up, accompanying with a negative thermal expansion. External hydrostatic pressure suppresses the resistivity jump progressively, coincident with the diminution of the  $\log T$  behavior. The low-temperature electronic specific-heat coefficient is extracted to be  $\sim 150 \text{ mJ K}^{-2} \text{ mol-fu}^{-1}$ , equivalent to  $\sim 50 \text{ mJ K}^{-2} \text{ mol-Ni}^{-1}$ , indicating an unusual heavy-electron correlated state. The novel heavy-electron state as well as the logarithmic temperature dependence of resistivity is explained in terms of the  $\text{Ni}^{3+}$  centered Kondo effect in the inner layer of the  $(\text{NdNiO}_3)_3$  trilayers.

PACS numbers: 72.80.Ga; 71.45.Lr; 75.30.Fv; 61.66.Fn; 74.10.+v

## I. INTRODUCTION

Perovskite-like nickelates possess similar crystal and electronic structures with those of high- $T_c$  cuprate superconductors<sup>1</sup>. It was earlier theoretically expected that high- $T_c$  superconductivity could be realized in layered nickelates with  $\text{NiO}_2$  sheets<sup>2-4</sup>, although the opposing ideas were later argued with addressing the differences<sup>5,6</sup>. Very recently, superconductivity at  $T_c = 9\text{-}15$  K was reported in the  $\text{Nd}_{0.8}\text{Sr}_{0.2}\text{NiO}_2$  single-crystalline thin films deposited on a  $\text{SrTiO}_3$  substrate<sup>7</sup>. The finding makes the layered nickelates a hot research topic in the condensed matter community<sup>8-18</sup>.

Most layered nickelates are structurally related to the Ruddlesden-Popper (RP) series,  $L_{n+1}\text{Ni}_n\text{O}_{3n+1}$  ( $L = \text{lanthanide elements}$ )<sup>19</sup>, which contains perovskite-type  $(\text{LNiO}_3)_n$  block-layers that are connected with a rock-salt-type  $\text{LO}$  layer. The average formal Ni valence in  $L_{n+1}\text{Ni}_n\text{O}_{3n+1}$  changes with  $n$ , being  $2+$ ,  $2.5+$ ,  $2.67+$ , and  $3+$ , respectively, at  $n = 1, 2, 3$ , and  $\infty$ . Furthermore, the apical oxygen atoms in between the  $\text{NiO}_2$  planes can be removed by a topochemical reduction, giving rise to the variant series  $L_{n+1}\text{Ni}_n\text{O}_{2n+2}$ <sup>20</sup> with the formal Ni valence of  $1.5+$ ,  $1.33+$ , and  $1+$ , respectively, for  $n = 2, 3$ , and  $\infty$ . Note that the Ni valence state in the trilayer  $L_4\text{Ni}_3\text{O}_8$  is mostly close to that in the

superconducting nickelate  $\text{Nd}_{0.8}\text{Sr}_{0.2}\text{NiO}_2$ . Therefore, the trilayer nickelates seem to be promising to realize superconductivity in the bulk form.

As the precursor of  $L_4\text{Ni}_3\text{O}_8$ ,  $L_4\text{Ni}_3\text{O}_{10}$  belong to the RP nickelates which contains trilayers of  $\text{NiO}_2$  sheets. So far, there are only three members in the family, with  $L = \text{La, Pr, and Nd}$ , respectively. Zhang and Greenblatt<sup>21</sup> earlier reported the synthesis, structure, and physical properties of  $L_4\text{Ni}_3\text{O}_{10-\delta}$ . Among them,  $\text{La}_4\text{Ni}_3\text{O}_{10}$  showed a metallic behavior with Pauli paramagnetism. For  $L = \text{Pr and Nd}$ , a metal-to-metal transition (MMT) was observed at 145 and 165 K, respectively, from the resistivity measurements. It was later indicated that the oxygen stoichiometry of  $\text{La}_4\text{Ni}_3\text{O}_{10\pm\delta}$  influenced the electronic properties<sup>22</sup>. A similar MMT at 140 K was also observed for the as-prepared  $\text{La}_4\text{Ni}_3\text{O}_{10.02}$  and reduced  $\text{La}_4\text{Ni}_3\text{O}_{9.78}$ , while the oxidized  $\text{La}_4\text{Ni}_3\text{O}_{10.12}$  did not show evidence of an MMT. Recently, the MMT in  $\text{La}_4\text{Ni}_3\text{O}_{10}$  was found to be accompanied with a structural response, featured with the expansion in the  $b$  axis, but without any change in the space group<sup>23,24</sup>. Note that the temperature dependence of magnetic susceptibility only shows a gradual decrease at the MMT<sup>22,24,25</sup>, apparently contradicting with the obvious jumps in the temperature dependence of resistivity and specific heat<sup>23,24</sup>.

The MMT was earlier attributed to a charge-density-wave (CDW) instability<sup>21</sup> or charge ordering<sup>22</sup>. The tight-binding bandstructure calculation study suggested two hidden one-dimensional Fermi surfaces which could be responsible for the charge density wave instability<sup>26</sup>. Recent angle resolved photoemission spectroscopy (ARPES) measurements<sup>1</sup> on  $\text{La}_4\text{Ni}_3\text{O}_{10}$  crystals indicated that, at the MMT, a gap of 20 meV opens in a flat band with strong  $d_{3z^2-r^2}$  orbital character, whereas no pseudogap was found in the band with the dominant  $d_{x^2-y^2}$  character. Nevertheless, the origin of the MMT remains elusive.

As the third member of  $\text{La}_4\text{Ni}_3\text{O}_{10}$ ,  $\text{Nd}_4\text{Ni}_3\text{O}_{10}$  has been rarely studied<sup>21,27</sup>. Albeit of the resistivity jump, no magnetic anomaly was observable, primarily due to the large magnetic contributions from the  $\text{Nd}^{3+}$  ions. Another motivation of this work is that  $\text{Nd}^{3+}$  has the smallest ionic radius among the  $L^{3+}$  ions<sup>28</sup>, which gives rise to the smallest tolerance factor ( $t = 0.932, 0.917$  and  $0.91$ , respectively, for  $\text{La}_4\text{Ni}_3\text{O}_{10}$ ,  $\text{Pr}_4\text{Ni}_3\text{O}_{10}$ , and  $\text{Nd}_4\text{Ni}_3\text{O}_{10}$ <sup>21</sup>). This would significantly influence the physical properties, like the case in the  $\text{LNiO}_3$  system<sup>29,30</sup>. In this paper we report the physical properties of  $\text{Nd}_4\text{Ni}_3\text{O}_{10-\delta}$ , particularly focusing on the MMT and the low-temperature properties. We found that the MMT is not only identified by the resistivity jump, but also characterized by a magnetic susceptibility drop, a specific-heat peak, and a nearly isotropic lattice contraction. Compared with the sister compound  $\text{La}_4\text{Ni}_3\text{O}_{10}$ , furthermore, the material shows a much larger electronic specific-heat coefficient and an enhanced  $\log T$  dependence in the low-temperature resistivity, indicating a novel heavy-fermion correlated electronic state in the title material.

## II. EXPERIMENTAL METHODS

$\text{Nd}_4\text{Ni}_3\text{O}_{10-\delta}$  polycrystalline samples were synthesized via high-temperature solid-state reactions. The source materials were  $\text{Nd}_2\text{O}_3$  (99.997%, Alfa Aesar) and  $\text{NiO}$  (99.998%, Alfa Aesar), which were mixed in the stoichiometric ratio ( $\text{Nd} : \text{Ni} = 4 : 3$ ). The ground mixture was first calcined at 1100 °C in oxygen atmosphere, holding for 36 hours. The resultant was found to be  $\text{Nd}_2\text{NiO}_4$ ,  $\text{Nd}_3\text{Ni}_2\text{O}_{7-\delta}$ , and  $\text{Nd}_4\text{Ni}_3\text{O}_{10-\delta}$ . In order to obtain the single-phase sample of  $\text{Nd}_4\text{Ni}_3\text{O}_{10-\delta}$ , the intermediate product (being reground and pressed into pellets) was sintered at 1100 °C for 48 hours in oxygen atmosphere (0.3-0.5 MPa at 1100 °C). The oxygen gas was generated by the decomposition of  $\text{Ag}_2\text{O}$  (99.7%, Aladdin) and, together with the sample pellets, appropriate amount of  $\text{Ag}_2\text{O}$  was put and sealed in an evacuated silica ampule. This high-temperature solid-state reaction led to single-phase sample of  $\text{Nd}_4\text{Ni}_3\text{O}_{10-\delta}$ . According to the previous literatures<sup>21,27</sup>, the sample prepared under an oxygen pressure of  $\sim 0.1$  MPa has oxygen deficiency with  $\delta \sim 0.15$ . The as-prepared sample was found to be stable in

air.

The sample was structurally examined by powder x-ray diffractions (XRD) using a PANalytical diffractometer (Empyrean Series 2) with a monochromatic  $\text{Cu-K}\alpha_1$  radiation. The crystal structure were refined by a Rietveld analysis using the GSAS package<sup>31</sup>. The fractional coordinates and the occupancies of the oxygen atoms were fixed according to the neutron diffraction result<sup>27</sup>, because neutron diffraction in general gives more accurate atomic positions for oxygen.

The temperature dependence of electrical resistivity and heat capacity was measured on a Quantum Design Physical Properties Measurement System (PPMS-9). In the resistivity measurement, the sample pellet was cut into a thin rectangular bar on which four parallel electrodes were made with silver paste. The dc magnetization was measured on a Quantum Design Magnetic Property Measurement System (MPMS3). The high-pressure resistivity was measured with the standard four-probe method in a palm-type cubic anvil cell (CAC) apparatus<sup>32</sup>. Glycerol was used as the pressure transmitting medium. The pressure values were estimated from the pressure-load calibration curve determined by observing the characteristic phase transitions of Bi (2.55, 2.7, 7.7 GPa), Sn (9.4 GPa), and Pb (13.4 GPa) at room temperature. It should be noted that the pressure values inside the CAC exhibit slight variations upon cooling, which has been well characterized in the previous work<sup>32</sup>.

## III. RESULTS AND DISCUSSION

### A. Crystal structure

Figure 1 shows the XRD and its Rietveld-analysis profile for the  $\text{Nd}_4\text{Ni}_3\text{O}_{10-\delta}$  sample studied in this paper. The Rietveld refinement was based on the structural model with the space group of  $P2_1/a$  and  $Z = 4$ <sup>27</sup>. The  $R$  factors and the goodness of the refinement are  $R_{\text{wp}} = 5.0\%$ ,  $R_p = 3.47\%$ , and  $\chi^2 = 1.94$ , respectively, suggesting reliability of the structural parameters fitted. The unit-cell parameters obtained are  $a = 5.36550(6)$  Å,  $b = 5.45462(6)$  Å,  $c = 27.4186(3)$  Å, and  $\beta = 90.318(1)^\circ$ , which are consistent with the previous report ( $a = 5.3675(2)$  Å,  $b = 5.4548(2)$  Å,  $c = 27.433(1)$  Å, and  $\beta = 90.312(2)^\circ$ <sup>27</sup>).

Shown in the inset of Fig. 1 is the crystal structure of  $\text{Nd}_4\text{Ni}_3\text{O}_{10-\delta}$ , which contains triple perovskite-type block layers in which the vertex-sharing  $\text{NiO}_6$  octahedra are distorted, twisted and tilted. There are four distinct crystallographic sites for Ni atoms, two of them are in the inner layer (IL), and others in the outer layer (OL). To assess the possible charge ordering state of  $\text{Ni}^{3+}-\text{Ni}^{2+}-\text{Ni}^{3+}$  in the trilayer<sup>22</sup>, we calculated the bond valence sum (BVS)<sup>33</sup> for the Ni ions, using the formula  $\sum \exp(\frac{R_0-d_{ij}}{0.37})$ , where  $R_0$  is 1.654 Å for a  $\text{Ni}^{2+}-\text{O}$  bond and  $d_{ij}$  are the measured interatomic distances between Ni cations and the coordinated oxygen

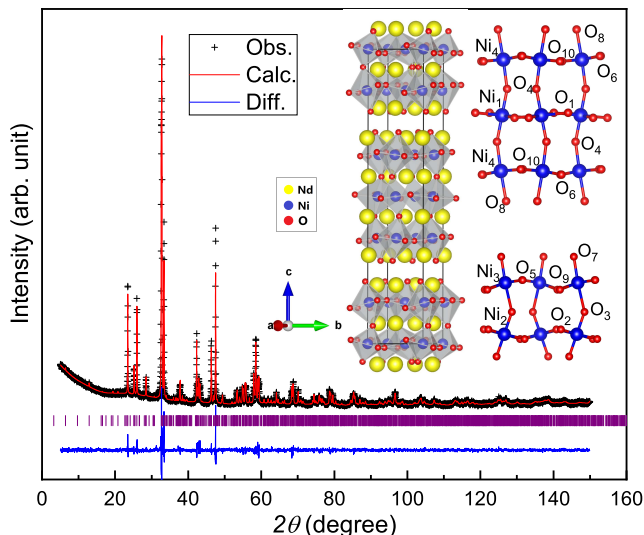


FIG. 1. Powder X-ray diffraction at room temperature and its Rietveld refinement profile of  $\text{Nd}_4\text{Ni}_3\text{O}_{10-\delta}$ . The insets show the crystal structure with vertex-sharing  $\text{NiO}_6$  octahedra.

anions. As is seen in Table I, the BVS values of the Ni atoms are about 2.6, consistent with the average formal Ni valence in  $\text{Nd}_4\text{Ni}_3\text{O}_{10}$ . However, there is no tendency of the charge ordering of  $\text{Ni}^{3+}-\text{Ni}^{2+}-\text{Ni}^{3+}$ . On the contrary, the Ni valence in the IL turns out to be higher. Similar results were reported for  $\text{La}_4\text{Ni}_3\text{O}_{10}$  and  $\text{Pr}_4\text{Ni}_3\text{O}_{10}$ <sup>23</sup>. Therefore, the possible extreme charge ordering scenario should be the case that the Ni valence in the IL is  $\text{Ni}^{3+}$  and, correspondingly, the formal Ni valence in the OLs could be 2.5+ for the stoichiometric  $\text{Nd}_4\text{Ni}_3\text{O}_{10}$ . Note that the interatomic distances between Ni and the apical oxygen,  $d_{\text{ap}}$ , are very different in the ILs and OLs. In the OLs,  $d_{\text{ap}}$  are obvious larger, reflecting a Jahn-Teller-like distortion or an orbital polarization<sup>34</sup>. The higher Ni valence in the ILs seems to be related to the shorter  $d_{\text{ap}}$ . It is of great interest to have a similar analysis for the low-temperature crystallographic data using neutron diffractions (such a work is under way). By the way, we also calculate the BVS values for the Nd ions. As listed in Table I, they are reasonably close to the conventional valence of  $\text{Nd}^{3+}$ , albeit of the difference in the coordination number.

### B. Electrical resistivity

Figure 2 shows the temperature dependence of resistivity for the as-prepared  $\text{Nd}_4\text{Ni}_3\text{O}_{10-\delta}$  polycrystalline sample. The  $\rho(T)$  behavior is basically metallic, and no sign of superconductivity is observed down to 0.16 K [see the inset of Fig. 2(a)]. One can immediately see a resistivity jump at  $T_{\text{MM}} = 161.3$  K, indicating a MMT which is basically consistent with the previous observation (the transition temperature, defined as the onset of the steep resistivity increase, was actually  $\sim 155$

K rather than 165 K in the previous report<sup>21</sup>). No thermal hysteresis is obvious, suggesting a second-order transition or a weakly first-order transition. The finite resistivity jump implies a partial bandgap opening at the Fermi level,  $E_F$ .

Noticeably, the  $\rho(T)$  data show an obvious upturn below 50 K, which approximately obeys a logarithmic temperature dependence, as shown in Fig. 2(b). The result is different from that of its sister compound  $\text{La}_4\text{Ni}_3\text{O}_{10-\delta}$ , the latter of which only shows a tiny (if not none) resistivity upturn<sup>1,21,22,24,25</sup>. In comparison, the low-temperature  $\rho(T)$  curve of  $\text{Pr}_4\text{Ni}_3\text{O}_{10.1}$  exhibits a clearer upturn<sup>35</sup>. This trend suggests that the enhanced resistivity upturn in  $\text{Nd}_4\text{Ni}_3\text{O}_{10-\delta}$  is associated with either the magnetism of  $\text{Nd}^{3+}$  ions or the smaller  $\text{Nd}^{3+}$  ions (compared with  $\text{La}^{3+}$ ). The latter gives rise to a strong lattice distortion and a consequent “more localized” electronic state akin to the case in  $\text{LNiO}_3$ <sup>29,30</sup>. In general, the energy level of Nd-4*f* electrons is far below the  $E_F$ , and the effective hybridization with the conduction bands is negligible. Note that a similar logarithmic temperature dependence of resistivity was seen in  $\text{NdNiO}_2$ <sup>7</sup> and  $\text{LaNiO}_2$ <sup>36</sup> thin films, which was recently interpreted in terms of the Ni-moment centered Kondo scattering<sup>15</sup>. Such a novel Kondo-like interaction was also theoretically discussed<sup>10,17</sup> and was recently demonstrated by the x-ray spectroscopy and density functional calculations for in  $\text{NdNiO}_2$  or  $\text{LaNiO}_2$ <sup>8</sup>. For  $\text{Nd}_4\text{Ni}_3\text{O}_{10-\delta}$  here, partial Ni-3*d* electrons possibly become localized below  $T_{\text{MM}}$  (akin to the site-selective Mottness<sup>37,38</sup>), which carry magnetic moments (see the following analysis). Such magnetic moments could serve as the Kondo-scattering centers, like the case in  $\text{NdNiO}_2$  or  $\text{LaNiO}_2$ , which may give rise to the low-temperature resistivity upturn.

### C. Magnetic properties

The magnetic measurement data of  $\text{Nd}_4\text{Ni}_3\text{O}_{10-\delta}$  were shown in Fig. 3. First of all, the field dependence of magnetization is essentially linear at  $T > 30$  K, indicating that the sample is free of ferromagnetic impurities. At 1.8 K, the  $M(H)$  curve is Brillouin function like and, at the lowest temperature down to 0.4 K, the magnetization almost saturates at  $\sim 5 \mu_B$  per formula unit (fu). The magnetic moment is severely reduced for the  $\text{Nd}^{3+}$  ions, since the theoretical ordered moment of a free  $\text{Nd}^{3+}$  ion is  $g_J J = 3.27 \mu_B$ , equivalent to  $13 \mu_B/\text{fu}$  for  $\text{Nd}_4\text{Ni}_3\text{O}_{10-\delta}$ . The reduction of the  $\text{Nd}^{3+}$  moment is commonly attributed to the crystalline-electric-field (CEF) effect. The CEF effect often gives rise to a  $J_{\text{eff}} = 1/2$  ground state for an odd number of 4*f* electrons. Indeed, the following specific-heat measurement confirms this scenario.

As shown in Fig. 3(b), the temperature dependence of susceptibility of  $\text{Nd}_4\text{Ni}_3\text{O}_{10-\delta}$  is Curie-Weiss (CW) like. The CW fit in the temperature range of  $165 \text{ K} < T <$

TABLE I. Bond valence sums (BVS) of Nd and Ni calculated with the related interatomic distances at 300 K in  $\text{Nd}_4\text{Ni}_3\text{O}_{10-\delta}$ . IL and OL are the abbreviations for inner layer and outer layer, respectively.

Nickel	site	$x$	$y$	$z$	$d(\text{Ni}-\text{O}_{\text{ap}})$			$d(\text{Ni}-\text{O}_{\text{eq}})$				BVS(Ni)					
Ni1 (IL1)	2b	0.0000	0.5000	0.5000	1.945	1.945		1.946	1.979	1.946	1.979	2.64					
Ni2 (IL2)	2a	0.0000	0.0000	0.0000	1.936	1.936		1.949	1.949	1.932	1.932	2.77					
Ni3 (OL1)	4e	-0.0157	0.0146	0.1406	1.994	2.117		1.956	2.042	1.867	1.877	2.58					
Ni4 (OL2)	4e	0.4988	0.0123	0.6409	2.118	1.989		1.882	1.897	1.993	1.951	2.59					
Neodymium	site	$x$	$y$	$z$	$d(\text{Nd}-\text{O}_{\text{up}})$			$d(\text{Nd}-\text{O}_{\text{mid}})$				$d(\text{Nd}-\text{O}_{\text{dn}})$				BVS(Nd)	
Nd1 (OL1)	4e	-0.0062	0.0177	0.3010	2.343			2.832	2.350	2.639	3.194	2.325	2.652	2.472	2.417	2.89	
Nd2 (OL2)	4e	0.5002	0.0111	0.8004	2.335			3.106	2.897	2.440	2.567	2.399	2.391	2.700	2.701	2.58	
Nd3 (IL1)	4e	0.0369	0.0069	0.4312	2.626	3.123	2.862	2.588	2.961	2.373	2.476	3.103	2.345	3.250	2.560	2.681	2.71
Nd4 (IL2)	4e	0.5153	-0.0092	0.9309	2.506	2.859	2.573	2.919	2.263	2.772	3.192	2.642	2.759	2.578	3.025	2.462	2.73

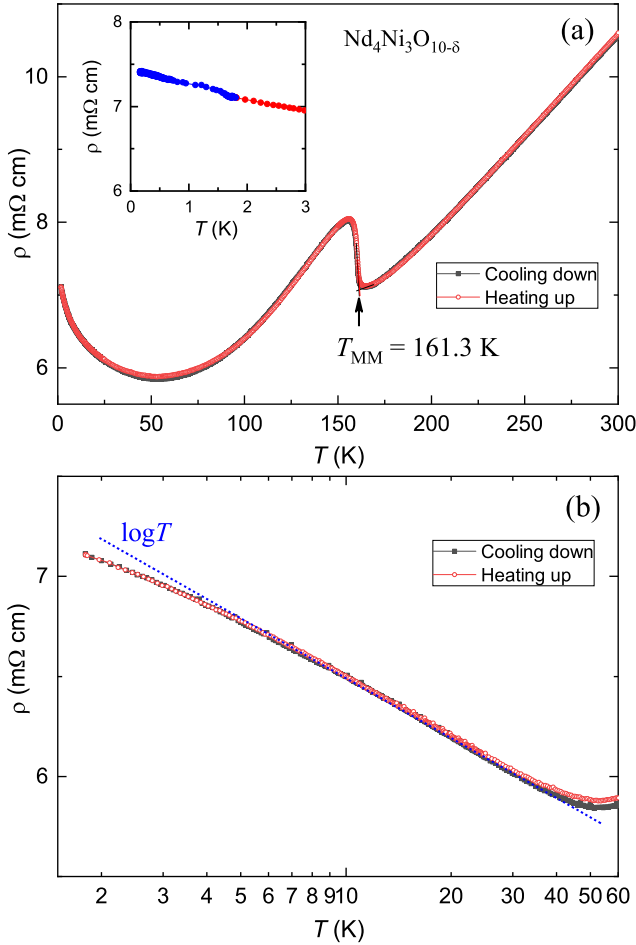


FIG. 2. Temperature (a) and logarithmic temperature (b) dependence of electrical resistivity of the  $\text{Nd}_4\text{Ni}_3\text{O}_{10-\delta}$  polycrystalline sample.

300 K using the formula  $\chi = \chi_0 + C/(T + \theta_W)$  yields a temperature-independent term  $\chi_0 = 0.0044 \text{ emu/mol-fu}$ , a Curie constant  $C = 6.43 \text{ emu K/mol-fu}$ , and a paramagnetic Weiss temperature  $\theta_W = 40.5 \text{ K}$ . With the fitted Curie constant, the effective local magnetic

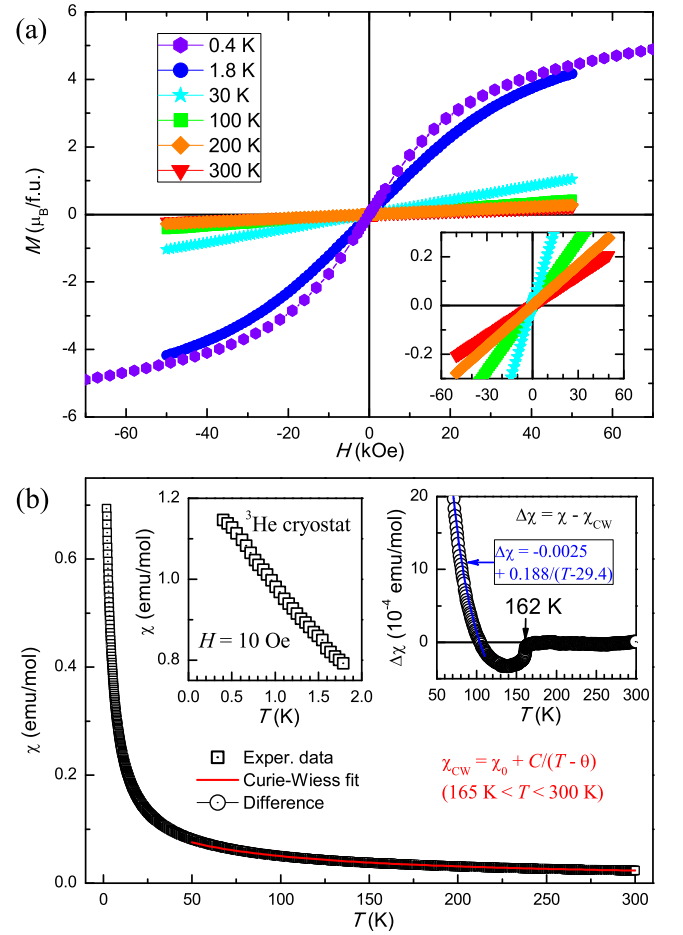


FIG. 3. (a) Magnetic field dependence of magnetization at some fixed temperature for  $\text{Nd}_4\text{Ni}_3\text{O}_{10-\delta}$ . The inset is a close-up for the high-temperature data, showing the linear dependence. (b) Temperature dependence of magnetic susceptibility under a magnetic field of  $H = 10 \text{ Oe}$  for  $\text{Nd}_4\text{Ni}_3\text{O}_{10-\delta}$ . The left inset shows the susceptibility down to 0.45 K using a  $^3\text{He}$  cryostat. The right inset plots the result of susceptibility subtraction with a Curie-Weiss fit.



moment is derived to be  $3.59 \mu_B/\text{Nd}^{3+}$ , close to the theoretical value of  $\text{Nd}^{3+}$  free ions ( $3.62 \mu_B$ ). This suggests that the magnetic moment from Ni at  $T > T_{\text{MM}}$ , if exists, is negligible. In spite of a significantly high value of  $\theta_W$ , which means substantial antiferromagnetic interactions between the  $\text{Nd}^{3+}$  moments, no magnetic transition associated with the  $\text{Nd}^{3+}$  moment is observed above 0.4 K. This could be due to a frustration effect, since the dominant magnetic coupling seems to be an indirect RKKY interaction. Finally,  $\chi_0$  is remarkably larger than the  $\chi$  value at 300 K for  $\text{La}_4\text{Ni}_3\text{O}_{10}$  ( $0.0018 \text{ emu/mol-fu}$ )<sup>21,22</sup>. The large value  $\chi_0$  should be mostly contributed from the exchange-enhanced Pauli paramagnetism and Van Vleck paramagnetism.

To detect a possible change in the magnetic susceptibility at the MMT, we made a subtraction using the CW-fit data as the reference. As shown in the right inset of Fig. 3(b), the subtraction reveals a susceptibility drop of  $\sim 3 \times 10^{-4} \text{ emu/mol-fu}$ . The susceptibility drop corresponds to a  $N(E_F)$  loss of  $\sim 9 \text{ states/eV}$ , suggesting a partial gap opening. Note that the susceptibility drop is so far exclusively observed for the MMT in the  $\text{La}_4\text{Ni}_3\text{O}_{10}$  family (only a gradual decrease at the MMT was seen for  $\text{La}_4\text{Ni}_3\text{O}_{10}$ <sup>22,24,25</sup>). Also noted is that, after the subtraction, the  $\chi(T)$  data below 140 K still show a CW-like behavior. This remaining CW term, with an effective local moment of  $\sim 1.2 \mu_B/\text{fu}$  (fitted with the data from 50 K to 120 K), could arise from the partial localized electronic states of Ni-3d electrons. This unusual state resembles the site-selective Mottness in  $\text{LNiO}_3$ <sup>38</sup>. As mentioned above, the Ni in the IL shows a higher BVS value, which implies dominant  $\text{Ni}^{3+}$  oxidation states in the ILs. Remember that  $\text{NdNiO}_3$  with  $\text{Ni}^{3+}$  oxidation states shows a metal-to-insulator transition at 201 K<sup>29</sup>. Thus the Ni-3d electronic states in the ILs are likely to be localized below  $T_{\text{MM}}$ . If this is the case, the MMT in the present system involves an interlayer charge ordering, in addition to the possible charge-transfer gap earlier proposed for  $\text{LNiO}_3$ <sup>29,30</sup>.

#### D. Specific heat

Figure 4 shows the temperature dependence of specific heat of the  $\text{Nd}_4\text{Ni}_3\text{O}_{10-\delta}$  sample. Remarkably, there is a sharp peak at 161 K, further confirming the bulk nature of the MMT. The entropy associated with the MMT is extracted to be  $2.8 \text{ J K}^{-1} \text{ mol-fu}^{-1}$ , which is about twice of that in  $\text{La}_4\text{Ni}_3\text{O}_{10}$ <sup>24</sup>. At  $T < 10 \text{ K}$ , the specific heat shows an upturn, as is clearly seen in the plot of  $C/T$  vs.  $T^2$  [inset of Fig. 4(a)]. In the temperature range of  $13 \text{ K} < T < 25 \text{ K}$ , a linear relation between  $C/T$  and  $T^2$  exists, reflecting the dominant contributions from the electronic part ( $\gamma T$ ) and the phonon part ( $\beta T^3$ ). The linear fit yields  $\gamma = 146 \text{ mJ K}^{-2} \text{ mol-fu}^{-1}$  and  $\beta = 1.22 \text{ mJ K}^{-4} \text{ mol-fu}^{-1}$ . The  $\gamma$  value is almost one order of magnitude larger than that in  $\text{La}_4\text{Ni}_3\text{O}_{10}$ <sup>24,25</sup>. This would suggest that the thermal effective mass  $m^*/m_0 \sim 26$ <sup>24,25</sup>,

suggesting a heavy-electron behavior. Finally, with the formula  $\theta_D = [(12/5)NR\pi^4/\beta]^{1/3}$ , where  $N$  denotes the number of atoms per formula unit ( $N = 17$ ), the Debye temperature  $\theta_D$  was estimated to be 300 K. This  $\theta_D$  value is in between those of the previous reports ( $256 \text{ K}$ <sup>25</sup> and  $384 \text{ K}$ <sup>24</sup>) for  $\text{La}_4\text{Ni}_3\text{O}_{10}$ .

To clarify the specific-heat tail below 10 K, we carried out the specific-heat measurement down to 0.5 K using a He-3 cryostat. The data are shown in Figs. 4(b,d). There is a broad hump at 0.5-2 K, which is commonly attributed to the Schottky anomaly from the  $\text{Nd}^{3+}$  ions<sup>39,40</sup>. We were able to separate the magnetic contributions by removing the electronic and phonon parts, which are plotted in Fig. 4(c). One sees an additional shoulder at around 5 K. This could be due to a complex Schottky anomaly (because of the complex CEF) and/or a possible Kondo effect<sup>41</sup>. The total magnetic entropy is  $17.5 \text{ J K}^{-1} \text{ mol}^{-1}$ , not far from an expected value of  $4R\ln 2 = 23.1 \text{ J K}^{-1} \text{ mol}^{-1}$  for a  $J_{\text{eff}} = 1/2$  ground state. The result is basically consistent with the low-lying doublet splitting of  $\text{Nd}^{3+}$  ions.

Under magnetic fields, the broad bump shifts to higher temperatures, as shown in Fig. 4(d), further confirming the Schottky anomaly scenario<sup>39,40</sup>. The specific heat at the lowest temperature of  $\sim 0.5 \text{ K}$  is mostly suppressed under a magnetic field of 8 T. This allows us to extract the electronic specific-heat coefficient independently. We thus made a polynomial extrapolation (roughly assuming that the magnetic contribution at 8 T is  $\delta T^5$ ) down to zero temperature, which yields  $(C/T)_{T \rightarrow 0} \approx 165 \text{ mJ K}^{-2} \text{ mol-fu}^{-1}$  [see the inset of Fig. 4(b)]. The result well agrees with the  $\gamma$  value obtained above.

#### E. Low-temperature XRD

To examine the possible structure change at the MMT, we conducted the low-temperature XRD measurement on  $\text{Nd}_4\text{Ni}_3\text{O}_{10-\delta}$ . The XRD data at 15 K can be well fitted on the basis of the identical crystal structure with the space group of  $P2_1/a$ . And we cannot distinguish the monoclinic-II phase ( $Z = 2$ ) from the monoclinic-I phase ( $Z = 4$ )<sup>42</sup>. Fig. 5(a) shows the XRD patterns at various temperatures. They are essentially the same except for slight peak shifts due to the changes in lattice parameters. The subtraction of the XRD data between 150 K and 170 K does not show any additional Bragg peaks. A similar result was reported in  $\text{Rb}_{1-\delta}\text{V}_2\text{Te}_2\text{O}_4$ <sup>43</sup> and  $\text{La}_4\text{Ni}_3\text{O}_{10}$  using synchrotron radiations<sup>23,24</sup>. Nevertheless, the possible CDW ordering cannot be ruled out due to the limitations of the XRD technique, and electron diffractions may be useful to clarify this issue in the future.

The lattice parameters were obtained by the Rietveld analysis, and its temperature dependence is shown in Figs. 5(b-d). At  $T \geq 170 \text{ K}$ , the lattice parameters decrease almost linearly with decreasing temperature. The volume expansion coefficient,  $\alpha_V = (1/V)(\partial V/\partial T)_P$ , is

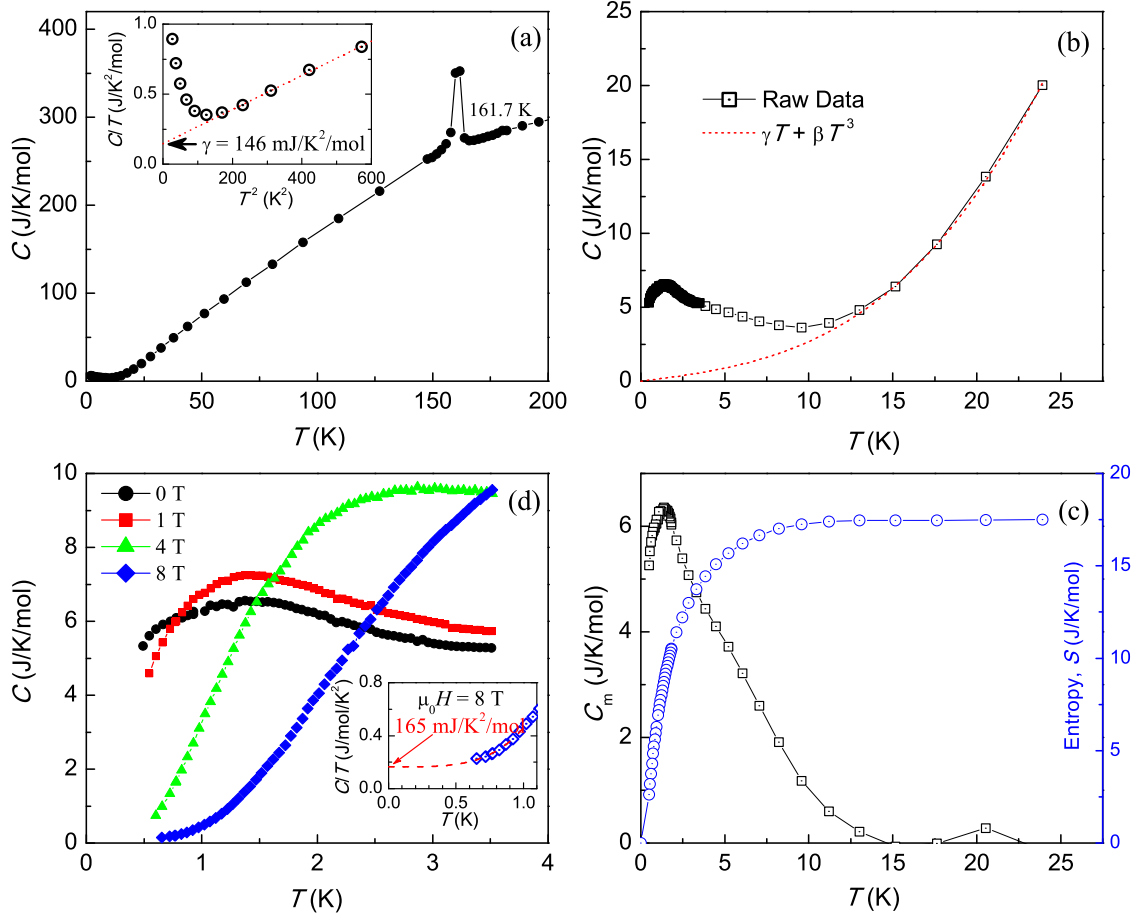


FIG. 4. Temperature dependence of specific heat for  $\text{Nd}_4\text{Ni}_3\text{O}_{10-\delta}$ . The insets of (a) and (d) plot  $C/T$  as functions of  $T^2$  and  $T$ , respectively, for extracting the electronic specific-heat coefficient. (c) Magnetic contributions of specific heat separated by the subtraction shown in (b). The right axis of (c) shows the magnetic entropy.

$4.3 \times 10^{-5} \text{ K}^{-1}$ . At  $T = 162 \text{ K}$ , a steep decrease is seen in all the unit-cell dimensions, resulting in a cell volume contraction of 0.08% at the MMT. The result is different with that of  $\text{La}_4\text{Ni}_3\text{O}_{10}$  in which only the  $b$  axis shows a 0.02% increase at the MMT<sup>23,24</sup>. The different structural response seems to be originated with the smaller tolerance factor in  $\text{Nd}_4\text{Ni}_3\text{O}_{10-\delta}$ .

Note that the lattice parameters *increase* with decreasing temperature below 50 K, indicating an anomalous negative thermal expansion (NTE) with an  $\alpha_V$  value of  $-2.7 \times 10^{-5} \text{ K}^{-1}$ . There are different types of mechanisms that may lead to a NTE<sup>44,45</sup>. In the present case, we note that the NTE phenomenon happens coincidentally with the resistivity upturn and even with the specific-heat upturn as described above. Thus the NTE is possibly associated with the “heavy-Fermion” behavior as well as the Schottky contributions<sup>44</sup>.

## F. High-pressure study

To study the pressure effect on the MMT and the low-temperature Kondo-like behavior in  $\text{Nd}_4\text{Ni}_3\text{O}_{10-\delta}$ , we have measured the temperature-dependent resistivity under various hydrostatic pressures up to 8 GPa using another single-phase sample. As shown in Fig. 6(a), the  $\rho(T)$  of  $\text{Nd}_4\text{Ni}_3\text{O}_{10-\delta}$  at ambient pressure displays a jump at  $T_{\text{MM}} \approx 162 \text{ K}$ . Above the  $T_{\text{MM}}$ , the resistivity increases linearly with temperature, while below  $T_{\text{MM}}$  a broad resistivity minimum centered at  $T_{\text{min}} \sim 70 \text{ K}$  appears with the resistivity upturn following a  $\log T$  dependence at low temperatures. Fig. 6(b) plots the  $T_{\text{MM}}$ , the resistivity jump  $\Delta\rho$ , and the  $T_{\text{min}}$  as functions of pressure  $P$ . With increasing  $P$ ,  $T_{\text{MM}}$  decrease mildly, from 162 K at 0 GPa to 130 K at 8 GPa with an initial slope of  $dT/dP \approx -10 \text{ K/GPa}$ , comparable to that of  $\text{La}_4\text{Ni}_3\text{O}_{10}$  ( $-6.9 \text{ K/GPa}$ )<sup>25</sup>. The gradual suppression of  $T_{\text{MM}}$  with pressure in  $\text{Nd}_4\text{Ni}_3\text{O}_{10-\delta}$  is also consistent with the observed lattice contraction at  $T_{\text{MM}}$  shown in Fig. 5, since high pressure usually stabilizes the smaller-volume phase. Meanwhile  $T_{\text{min}}$  decreases rapidly at low

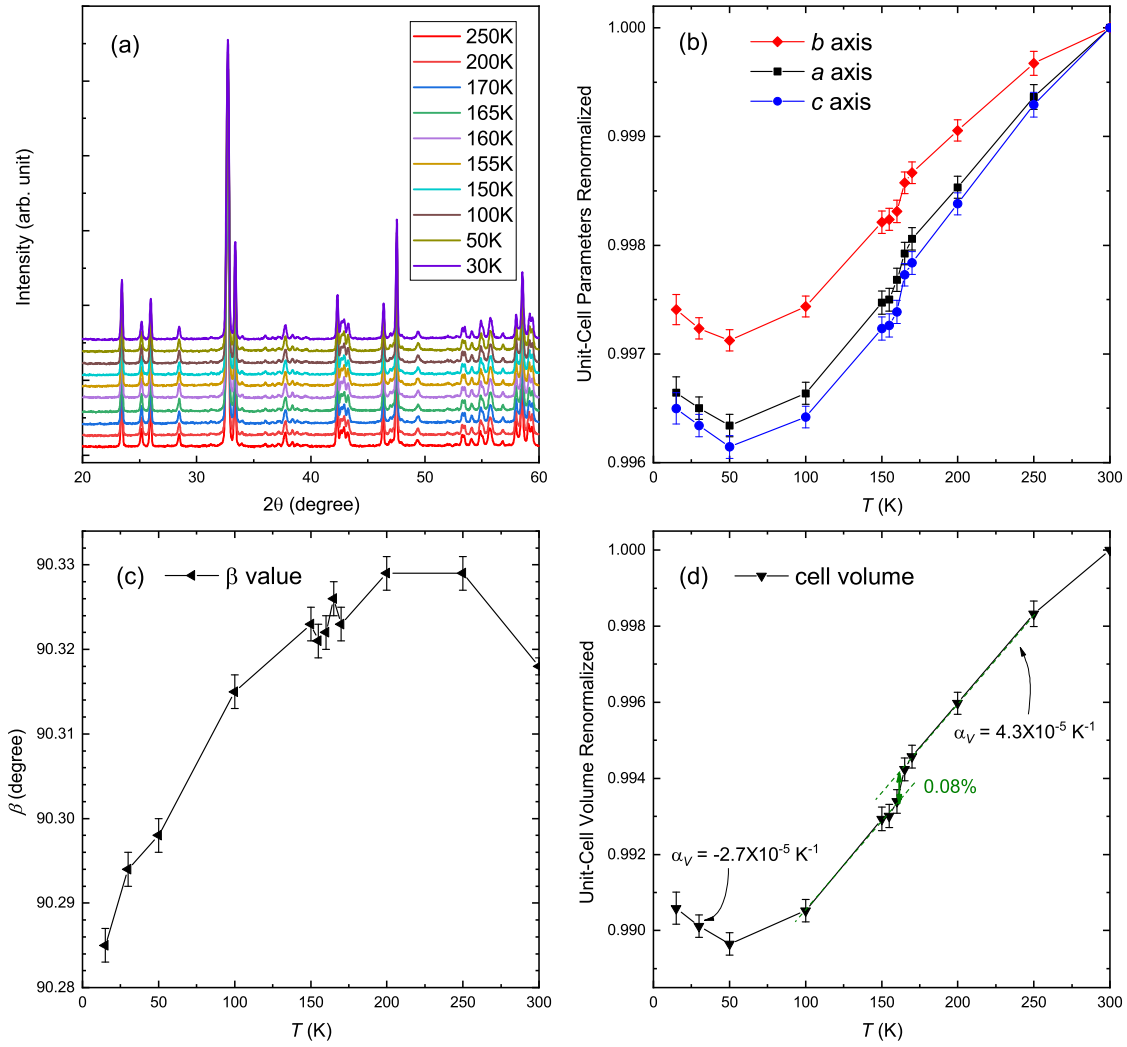


FIG. 5. (a) Low-temperature X-ray diffractions for  $\text{Nd}_4\text{Ni}_3\text{O}_{10-\delta}$ . (b) Temperature dependence of renormalized lattice parameters  $a$ ,  $b$ , and  $c$ , which shows a lattice contraction at 162 K and lattice expansions below 50 K. (c,d) Temperature dependence of the  $\beta$  value and the renormalized unit-cell volume, respectively.

pressures. And it tends to remain unchanged ( $\sim 26$  K) at higher pressures similar to the low-temperature  $\rho(T)$  behavior of  $\text{La}_4\text{Ni}_3\text{O}_{10}$  ( $T_{\min} = 20$  K)<sup>24</sup>. The resistivity jump  $\Delta\rho$  is mostly sensitive to pressure, and it diminishes much faster than  $T_{\text{MM}}$  and  $T_{\min}$  do. From these trends, it is very likely that the MMT will be eliminated completely at a finite temperature without approaching a quantum critical point.

Fig. 6(c) shows a semi-logarithmic plot for the high-pressure low-temperature resistivity data. At ambient pressure the  $\rho(T)$  data exhibit a logarithmic-temperature dependence below 50 K. At  $P \geq 1$  GPa, the Kondo-like resistivity upturn is remarkably reduced, coincident with the suppression of the MMT. The result suggests that the MMT may be the prerequisite of the Kondo-like electron-correlated behavior, in line with the  $\text{Ni}^{3+}$  centered Kondo effect mentioned above. Note that the weak upturn of  $\rho(T)$  at higher pressures is very similar to that of

$\text{La}_4\text{Ni}_3\text{O}_{10}$ <sup>24</sup>. This suggests that the heavy-electron behavior in  $\text{Nd}_4\text{Ni}_3\text{O}_{10-\delta}$  disappears largely under high pressures.

## G. Discussion

From the results above, one sees that the MMT in  $\text{Nd}_4\text{Ni}_3\text{O}_{10-\delta}$  bears both similarities and differences with that of its sister compound  $\text{La}_4\text{Ni}_3\text{O}_{10}$ . Both materials show a resistivity jump, a specific-heat anomaly, and a structural response at the MMT. Nevertheless, unlike  $\text{La}_4\text{Ni}_3\text{O}_{10}$  which shows a continuous expansion in the  $b$  axis at the MMT<sup>23,24</sup>,  $\text{Nd}_4\text{Ni}_3\text{O}_{10-\delta}$  exhibits a nearly isotropic lattice contraction. Also  $\text{Nd}_4\text{Ni}_3\text{O}_{10-\delta}$  exclusively exhibits an obvious magnetic susceptibility drop, indicating a significant loss of  $N(E_F)$ . The result suggests different types of charge ordering and/or

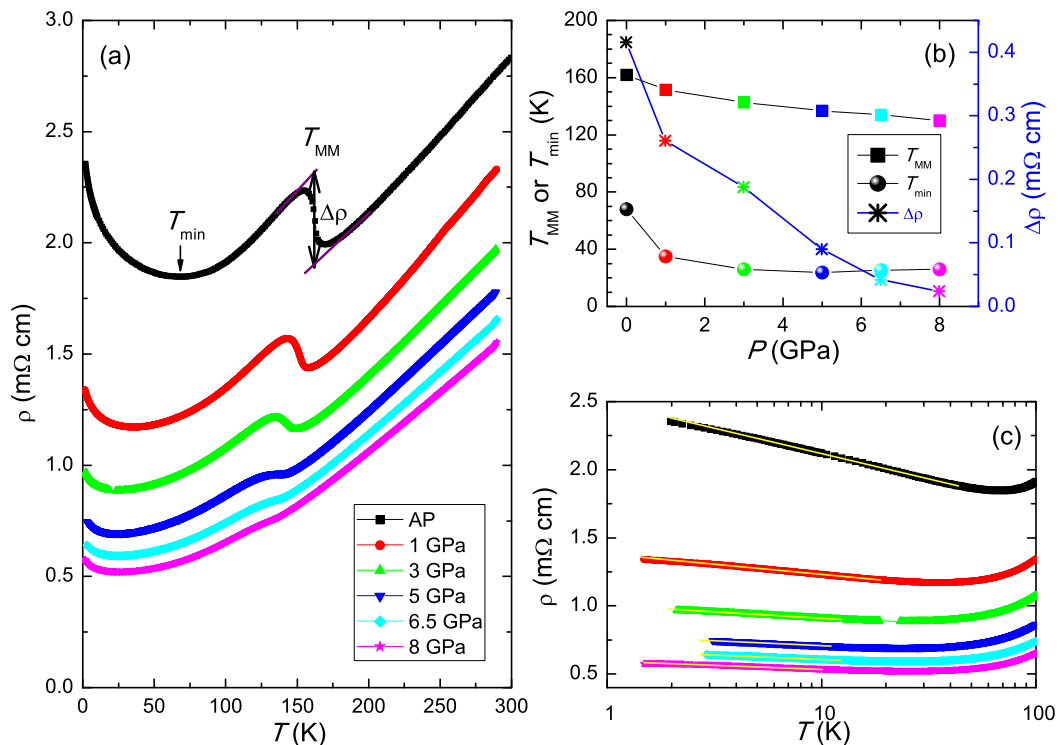


FIG. 6. (a) Temperature-dependent resistivity of  $\text{Nd}_4\text{Ni}_3\text{O}_{10-\delta}$  under various hydrostatic pressures up to 8 GPa. (b) The metal-to-metal transition temperature ( $T_{\text{MM}}$ ), the resistivity jump at  $T_{\text{MM}}$  ( $\Delta\rho$ , right axis), and the temperature at which the resistivity shows a minimum ( $T_{\min}$ ) are plotted as functions of pressure. (c) Logarithmic temperature dependence of resistivity at low temperatures and under pressures. The yellow straight lines are guides to the eyes.

CDW among the trilayer nickelate family, primarily due to the different tolerance factor as mentioned above. The similar “ionic size effect” exists in perovskite-type nickelates  $\text{LNiO}_3$ <sup>29</sup>. An additional work related is that, in ultrathin  $\text{LaNiO}_3$  films, the strain from the substrates governs the lattice distortion, which produces an emergent charge-ordered ground state<sup>46</sup>.

Owing to the higher Ni valence in the IL of the  $(\text{NdNiO}_3)_3$  trilayers, as indicated from the BVS value, the inner perovskite-like layer may undergo a metal-to-insulator transition like the case in  $\text{NdNiO}_3$ <sup>29,37,38</sup>. Meanwhile, the OLs possibly remain to be metallic. The resistivity jump and the magnetic susceptibility drop at the MMT support this picture. Additionally, a very recent work on  $\text{Pr}_4\text{Ni}_3\text{O}_{10}$ <sup>47</sup> revealed metallic and semi-conducting behaviors just below the MMT, respectively, for electric current flowing in the  $ab$  plane and along the  $c$  axis. Considered the similarity between  $\text{Pr}_4\text{Ni}_3\text{O}_{10}$  and  $\text{Nd}_4\text{Ni}_3\text{O}_{10}$ , a similar anisotropy probably exists in  $\text{Nd}_4\text{Ni}_3\text{O}_{10}$  also, which corroborates that the electronic state in the IL becomes largely localized below the MMT. In this context, the low-temperature state of  $\text{Nd}_4\text{Ni}_3\text{O}_{10}$  may be a natural metal/insulator/metal superlattice of nickelate, first proposed by Chaloupka and Khaliullin<sup>3</sup>, in which orbital order and possible superconductivity were expected.

Importantly, the dominant  $\text{Ni}^{3+}$  ions in the insulating

ILs carry a magnetic moment, which may serve as the Kondo-scattering centers. Note that the itinerant conduction electrons are also from the Ni-3d electrons (yet in the OLs). The situation is something like the site-selective Mott phase in  $\text{LNiO}_3$  in which the  $d$  electrons on part of the  $\text{Ni}^{3+}$  ions are localized while the  $d$  electrons on other  $\text{Ni}^{3+}$  ions form a singlet with holes on the surrounding oxygen ions.<sup>38</sup> With this picture in mind, the logarithmic temperature dependence of resistivity below 50 K and the heavy-electron behavior in  $\text{Nd}_4\text{Ni}_3\text{O}_{10-\delta}$  can be understood in terms of the novel Kondo scattering.

#### IV. CONCLUDING REMARKS

In summary, the trilayer nickelate  $\text{Nd}_4\text{Ni}_3\text{O}_{10-\delta}$  exhibits a metal-to-metal transition at 162 K, featured by a resistivity jump, a susceptibility drop, a specific-heat peak, and a nearly isotropic lattice contraction. The magnetic susceptibility drop is observed for the first time in the trilayer nickelate family. Besides,  $\text{Nd}_4\text{Ni}_3\text{O}_{10-\delta}$  shows a distinguishable logarithmic temperature dependence below 50 K. Furthermore, compared with  $\text{La}_4\text{Ni}_3\text{O}_{10}$ ,  $\text{Nd}_4\text{Ni}_3\text{O}_{10-\delta}$  possesses a much larger electronic specific-heat coefficient. The heavy-electron behavior is possibly associated with the localized



$\text{Ni}^{3+}$  states in the inner layer of the  $(\text{NdNiO}_3)_3$  block. The different physical properties between  $\text{La}_4\text{Ni}_3\text{O}_{10}$  and  $\text{Nd}_4\text{Ni}_3\text{O}_{10}$  highlight the role of the tolerance factor in controlling the electronic state as well as the lattice distortion.

At least phenomenologically, the MMT of  $\text{Nd}_4\text{Ni}_3\text{O}_{10-\delta}$  bears similarities to those of the Fe-based<sup>48</sup> and Ti-based<sup>49,50</sup> pnictides. The latter are associated with a density-wave instability, and suppression of the density-wave ordering gives rise to superconductivity<sup>48,51,52</sup>. External hydrostatic pressure tends to quench the MMT at a finite temperature in  $\text{Nd}_4\text{Ni}_3\text{O}_{10-\delta}$ , thus a quantum critical point is unlikely, and superconductivity was not observed down to 1.6 K. Nevertheless, superconductivity could be hopefully realized in the nickelates through a suitable chemical substitution in the future.

## ACKNOWLEDGMENTS

We thank Yi-feng Yang for helpful discussions. The work at ZJU was supported by the National Key Research and Development Program of China (2017YFA0303002 and 2016YFA0300202) and the Fundamental Research Funds for the Central Universities of China. The work at IOPCAS was supported by the National Key Research and Development Program of China (2018YFA0305700), the National Natural Science Foundation of China (11834016, 11874400), Beijing Natural Science Foundation (Z190008), the Key Research Program of Frontier Sciences of the Chinese Academy of Sciences (QYZDB-SSW-SLH013), and the CAS Interdisciplinary Innovation Team.

- 
- \* corresponding author: ghcao@zju.edu.cn
- <sup>1</sup> H. X. Li, X. Q. Zhou, T. Nummy, J. J. Zhang, V. Pardo, W. E. Pickett, J. F. Mitchell, and D. S. Dessau, Fermiology and electron dynamics of trilayer nickelate  $\text{La}_4\text{Ni}_3\text{O}_{10}$ , *Nature Communications* **8**, 704 (2017).
  - <sup>2</sup> V. I. Anisimov, D. Bukhvalov, and T. M. Rice, Electronic structure of possible nickelate analogs to the cuprates, *Phys. Rev. B* **59**, 7901 (1999).
  - <sup>3</sup> J. c. v. Chaloupka and G. Khaliullin, Orbital Order and Possible Superconductivity in  $\text{LaNiO}_3/\text{LaMO}_3$  Superlattices, *Phys. Rev. Lett.* **100**, 016404 (2008).
  - <sup>4</sup> A. S. Botana, V. Pardo, and M. R. Norman, Electron doped layered nickelates: Spanning the phase diagram of the cuprates, *Phys. Rev. Materials* **1**, 021801 (2017).
  - <sup>5</sup> K.-W. Lee and W. E. Pickett, Infinite-layer  $\text{LaNiO}_2$ :  $\text{Ni}^{1+}$  is not  $\text{Cu}^{2+}$ , *Phys. Rev. B* **70**, 165109 (2004).
  - <sup>6</sup> M. J. Han, X. Wang, C. A. Marianetti, and A. J. Millis, Dynamical Mean-Field Theory of Nickelate Superlattices, *Phys. Rev. Lett.* **107**, 206804 (2011).
  - <sup>7</sup> D. Li, K. Lee, B. Y. Wang, M. Osada, S. Crossley, H. R. Lee, Y. Cui, Y. Hikita, and H. Y. Hwang, Superconductivity in an infinite-layer nickelate, *Nature* **572**, 624 (2019).
  - <sup>8</sup> M. Hepting, D. Li, C. J. Jia, H. Lu, E. Paris, Y. Tseng, X. Feng, M. Osada, E. Been, Y. Hikita, Y. D. Chuang, Z. Hussain, K. J. Zhou, A. Nag, M. Garcia-Fernandez, M. Rossi, H. Y. Huang, D. J. Huang, Z. X. Shen, T. Schmitt, H. Y. Hwang, B. Moritz, J. Zaanen, T. P. Devereaux, and W. S. Lee, Electronic structure of the parent compound of superconducting infinite-layer nickelates, *Nat. Mater.* **xx**, xxxxxx (2020).
  - <sup>9</sup> A. S. Botana and M. R. Norman, Similarities and Differences between  $\text{LaNiO}_2$  and  $\text{CaCuO}_2$  and Implications for Superconductivity, *Phys. Rev. X* **10**, 011024 (2020).
  - <sup>10</sup> M.-Y. Choi, K.-W. Lee, and W. E. Pickett, Role of  $4f$  states in infinite-layer  $\text{NdNiO}_2$ , *Phys. Rev. B* **101**, 020503 (2020).
  - <sup>11</sup> P. Werner and S. Hoshino, Nickelate superconductors: Multiorbital nature and spin freezing, *Phys. Rev. B* **101**, 041104 (2020).
  - <sup>12</sup> L.-H. Hu and C. Wu, Two-band model for magnetism and superconductivity in nickelates, *Phys. Rev. Research* **1**, 032046 (2019).
  - <sup>13</sup> Y. Nomura, M. Hirayama, T. Tadano, Y. Yoshimoto, K. Nakamura, and R. Arita, Formation of a two-dimensional single-component correlated electron system and band engineering in the nickelate superconductor  $\text{NdNiO}_2$ , *Phys. Rev. B* **100**, 205138 (2019).
  - <sup>14</sup> P. Jiang, L. Si, Z. Liao, and Z. Zhong, Electronic structure of rare-earth infinite-layer  $\text{RNiO}_2$  ( $R = \text{La}, \text{Nd}$ ), *Phys. Rev. B* **100**, 201106 (2019).
  - <sup>15</sup> G.-M. Zhang, Y.-f. Yang, and F.-C. Zhang, Self-doped Mott insulator for parent compounds of nickelate superconductors, *Phys. Rev. B* **101**, 020501 (2020).
  - <sup>16</sup> Z. Liu, Z. Ren, W. Zhu, Z. F. Wang, and J. Yang, Electronic and Magnetic Structure of Infinite-layer  $\text{NdNiO}_2$ : Trace of Antiferromagnetic Metal, *arXiv* **1912**, 01332v2 (2019).
  - <sup>17</sup> Y.-H. Zhang and V. Ashvin, Type II  $t - J$  model in superconducting nickelate  $\text{Nd}_{1-x}\text{Sr}_x\text{NiO}_2$ , *arXiv* **1909**, 12865v2 (2019).
  - <sup>18</sup> Q. Li, C. He, J. Si, X. Zhu, Y. Zhang, and H.-H. Wen, Absence of superconductivity in bulk  $\text{Nd}_{1-x}\text{Sr}_x\text{NiO}_2$ , *arXiv* **1911**, 02420 (2019).
  - <sup>19</sup> K. Sreedhar, M. McElfresh, D. Perry, D. Kim, P. Metcalf, and J. M. Honig, Low-temperature electronic properties of the  $\text{La}_{n+1}\text{Ni}_n\text{O}_{3n+1}$  ( $n = 2, 3$ , and  $\infty$ ) system: evidence for a crossover from fluctuating-valence to Fermi-liquid-like behavior, *Journal of Solid State Chemistry* **110**, 208 (1994).
  - <sup>20</sup> P. Lacorre, Passage from T-type to  $\text{T}'$ -type arrangement by reducing  $\text{R}_4\text{Ni}_3\text{O}_{10}$  to  $\text{R}_4\text{Ni}_3\text{O}_8$  ( $R = \text{La}, \text{Pr}, \text{Nd}$ ), *Journal of Solid State Chemistry* **97**, 495 (1992).
  - <sup>21</sup> Z. Zhang and M. Greenblatt, Synthesis, structure, and properties of  $\text{Ln}_4\text{Ni}_3\text{O}_{10-\delta}$  ( $\text{Ln} = \text{La}, \text{Pr}$ , and  $\text{Nd}$ ), *Journal of Solid State Chemistry* **117**, 236 (1995).
  - <sup>22</sup> M. D. Carvalho, M. M. Cruz, A. Wattiaux, J. M. Bassat, F. M. A. Costa, and M. Godinho, Influence of oxygen stoichiometry on the electronic properties of  $\text{La}_4\text{Ni}_3\text{O}_{10+\delta}$ , *Journal of Applied Physics* **88**, 544 (2000).
  - <sup>23</sup> J. Zhang, H. Zheng, Y.-S. Chen, Y. Ren, M. Yonemura,

- A. Huq, and J. F. Mitchell, High oxygen pressure floating zone growth and crystal structure of the layered nickelates  $R_4Ni_3O_{10}$  ( $R=La, Pr$ ), arXiv **1904**, 10048 (2019).
- <sup>24</sup> S. Kumar, Ø. Fjellvåg, A. O. Sjøstad, and H. Fjellvåg, Physical properties of Ruddlesden-Popper ( $n = 3$ ) nickelate:  $La_4Ni_3O_{10}$ , Journal of Magnetism and Magnetic Materials **496**, 165915 (2020).
  - <sup>25</sup> G. Wu, J. J. Neumeier, and M. F. Hundley, Magnetic susceptibility, heat capacity, and pressure dependence of the electrical resistivity of  $La_3Ni_2O_7$  and  $La_4Ni_3O_{10}$ , Phys. Rev. B **63**, 245120 (2001).
  - <sup>26</sup> D. K. Seo, W. Liang, M. H. Whangbo, Z. Zhang, and M. Greenblatt, Electronic Band Structure and Madelung Potential Study of the Nickelates  $La_2NiO_4$ ,  $La_3Ni_2O_7$ , and  $La_4Ni_3O_{10}$ , Inorganic Chemistry **35**, 6396 (1996).
  - <sup>27</sup> A. Olafsen, H. Fjellvåg, and B. C. Hauback, Crystal structure and properties of  $Nd_4Co_3O_{10+\delta}$  and  $Nd_4Ni_3O_{10-\delta}$ , Journal of Solid State Chemistry **151**, 46 (2000).
  - <sup>28</sup> R. D. Shannon, Revised effective ionic radii and systematic studies of interatomic distances in halides and chalcogenides, Acta Crystallographica Section A **32**, 751 (1976).
  - <sup>29</sup> J. B. Torrance, P. Lacorre, A. I. Nazzari, E. J. Ansaldo, and C. Niedermayer, Systematic study of insulator-metal transitions in perovskites  $RNiO_3$  ( $R=Pr, Nd, Sm, Eu$ ) due to closing of charge-transfer gap, Phys. Rev. B **45**, 8209 (1992).
  - <sup>30</sup> M. L. Medarde, Structural, magnetic and electronic properties of  $RNiO_3$  perovskites ( $R =$  rare earth), Journal of Physics: Condensed Matter **9**, 1679 (1997).
  - <sup>31</sup> B. H. Toby, EXPGUI, a graphical user interface for GSAS, J. Appl. Crystallogr. **34**, 210 (2001).
  - <sup>32</sup> J. G. Cheng, K. Matsubayashi, S. Nagasaki, T. Hisada, A. Hirayama, M. Hedo, H. Kagi, and Y. Uwatoko, Integrated-fin gasket for palm cubic-anvil high pressure apparatus, Rev. Sci. Instrum. **85**, 093907 (2014).
  - <sup>33</sup> I. D. Brown and D. Altermatt, Bond-valence parameters obtained from a systematic analysis of the inorganic crystal structure database, Acta Crystallographica Section B **41**, 244 (1985).
  - <sup>34</sup> A. S. Disa, F. J. Walker, S. Ismail-Beigi, and C. H. Ahn, Research Update: Orbital polarization in  $LaNiO_3$ -based heterostructures, APL Materials **3**, 062303 (2015).
  - <sup>35</sup> J. M. Bassat, C. Allançon, P. Odier, J. P. Loup, M. D. Carvalho, and A. Wattiaux, Electronic properties of  $Pr_4Ni_3O_{10\pm\delta}$ , European Journal of Solid State and Inorganic Chemistry **35**, 173 (1998).
  - <sup>36</sup> A. Ikeda, Y. Krockenberger, H. Irie, M. Naito, and H. Yamamoto, Direct observation of infinite  $NiO_2$  planes in  $LaNiO_2$  films, Applied Physics Express **9**, 061101 (2016).
  - <sup>37</sup> M. K. Stewart, J. Liu, M. Kareev, J. Chakhalian, and D. N. Basov, Mott Physics near the Insulator-To-Metal Transition in  $NdNiO_3$ , Phys. Rev. Lett. **107**, 176401 (2011).
  - <sup>38</sup> H. Park, A. J. Millis, and C. A. Marianetti, Site-Selective Mott Transition in Rare-Earth-Element Nickelates, Phys. Rev. Lett. **109**, 156402 (2012).
  - <sup>39</sup> J. G. Cheng, Y. Sui, Z. N. Qian, Z. G. Liu, J. P. Miao, X. Q. Huang, Z. Lu, Y. Li, X. J. Wang, and W. H. Su, Schottky-like anomaly in the low-temperature specific heat of single-crystal  $NdMnO_3$ , Solid State Commun. **134**, 381 (2005).
  - <sup>40</sup> L. Xie and X. G. Su, T. S. Li, Magnetic field dependence of Schottky anomaly in the specific heats of stripe-ordered superconductors  $La_{1.6-x}Nd_{0.4}Sr_{-x}CuO_4$ , Physica C-Superconductivity and its Applications **480**, 14 (2012).
  - <sup>41</sup> V. T. Rajan, J. H. Lowenstein, and N. Andrei, Thermodynamics of the Kondo Model, Phys. Rev. Lett. **49**, 497 (1982).
  - <sup>42</sup> D. Puggioni and J. M. Rondinelli, Crystal structure stability and electronic properties of the layered nickelate  $La_4Ni_3O_{10}$ , Phys. Rev. B **97**, 115116 (2018).
  - <sup>43</sup> A. Ablimit, Y.-L. Sun, H. Jiang, S.-Q. Wu, Y.-B. Liu, and G.-H. Cao, Weak metal-metal transition in the vanadium oxytelluride  $Rb_{1-\delta}V_2Te_2O$ , Phys. Rev. B **97**, 214517 (2018).
  - <sup>44</sup> G. D. Barrera, J. A. O. Bruno, T. H. K. Barron, and N. L. Allan, Negative thermal expansion, Journal of Physics: Condensed Matter **17**, R217 (2005).
  - <sup>45</sup> J. Chen, L. Hu, J. Deng, and X. Xing, Negative thermal expansion in functional materials: controllable thermal expansion by chemical modifications, Chemical Society Reviews **44**, 3522 (2015).
  - <sup>46</sup> J. Chakhalian, J. M. Rondinelli, J. Liu, B. A. Gray, M. Kareev, E. J. Moon, N. Prasai, J. L. Cohn, M. Varela, I. C. Tung, M. J. Bedzyk, S. G. Altendorf, F. Strigari, B. Dabrowski, L. H. Tjeng, P. J. Ryan, and J. W. Freeland, Asymmetric Orbital-Lattice Interactions in Ultrathin Correlated Oxide Films, Phys. Rev. Lett. **107**, 116805 (2011).
  - <sup>47</sup> S. Huangfu, G. D. Jakub, X. Zhang, O. Blacque, P. Puphal, E. Pomjakushina, F. O. v. Rohr, and A. Schilling, Anisotropic character of the metal-to-metal transition in  $Pr_4Ni_3O_{10}$ , arXiv **2001**, 05916 (2020).
  - <sup>48</sup> G. Wu, H. Chen, T. Wu, Y. L. Xie, Y. J. Yan, R. H. Liu, X. F. Wang, J. J. Ying, and X. H. Chen, Different resistivity response to spin-density wave and superconductivity at 20 K in  $Ca_{1-x}Na_xFe_2As_2$ , Journal of Physics: Condensed Matter **20**, 422201 (2008).
  - <sup>49</sup> T. C. Ozawa, R. Pantoja, I. Enos A. Axtell, and S. M. Kauzlarich, Powder Neutron Diffraction Studies of  $Na_2Ti_2Sb_2O$  and Its Structure Property Relationships, J. Solid State Chem. **153**, 275 (2000).
  - <sup>50</sup> X. F. Wang, Y. J. Yan, J. J. Ying, Q. J. Li, M. Zhang, N. Xu, and X. H. Chen, Structure and physical properties for a new layered pnictide-oxide:  $BaTi_2As_2O$ , J. Phys.: Condens. Matter **22**, 075702 (2010).
  - <sup>51</sup> P. Doan, M. Gooch, Z. Tang, B. Lorenz, A. Möller, J. Tapp, P. C. W. Chu, and A. M. Guloy,  $Ba_{1-x}Na_xTi_2Sb_2O$  ( $0.0 \leq x \leq 0.33$ ): A Layered Titanium-Based Pnictide Oxide Superconductor, J. Am. Chem. Soc. **134**, 16520 (2012).
  - <sup>52</sup> H.-F. Zhai, W.-H. Jiao, Y.-L. Sun, J.-K. Bao, H. Jiang, X.-J. Yang, Z.-T. Tang, Q. Tao, X.-F. Xu, Y.-K. Li, C. Cao, J.-H. Dai, Z.-A. Xu, and G.-H. Cao, Superconductivity, charge- or spin-density wave, and metal-nonmetal transition in  $BaTi_2(Sb_{1-x}Bi_x)_2O$ , Phys. Rev. B **87**, 100502 (2013).